SAR DESPECKLING FILTERS IN ULTRASOUND IMAGING

JING YI JIN[†], GLAUBER T. SILVA[‡] and ALEJANDRO C. FRERY[⋆]

† *University of Illinois at Urbana-Champaign, Department of Computer Science*
1304 W. Springfield Avenue, Urbana, IL 61801, USA
jingjin@uiuc.edu

‡ *Universidade Federal de Pernambuco, Centro de Informática*
CP 7851
50732-970 Recife, PE – Brazil
gjfts@cin.ufpe.br

⋆ *Universidade Federal de Alagoas, Departamento de Tecnologia da Informação*
Campus A. C. Simões, BR 104 km 14, Bl. 12
57072-970 Maceió, AL – Brazil
frery@tci.ufal.br

***Abstract*— Ultrasonics is a widely used technique in medical imaging, due to its non-invasive nature and its capability of forming real-time portraits of hidden targets. In this technique, pulse-echo ultrasonic waves are sent to the investigated medium and the backscattered waves provide the information for image formation. However, the coherent nature of the waves results in the appearance of speckle noise. This phenomenon is common to laser, sonar and synthetic aperture radar (SAR) imagery, and is the result of interference between the scattered waves. Many filters have been proposed for alleviating this noise, especially in remote sensing applications. Some of these filters (Mean, Median, Lee, Frost and Gaussian MAP) are reviewed and applied to ultrasound B-scan images, along with a non-linear technique based on computing the median on the binary slices of the data. The performance of these techniques is assessed both quantitatively (regarding noise suppression and radiometric preservation) and qualitatively (through perceptual contrast and edge preservation).**

***Keywords*— Image processing, Speckle, Ultrasound.**

I. INTRODUCTION

The importance of ultrasound imaging in medicine and other fields of application is enormous. It is estimated that more than one out of every four medical diagnostic imaging studies in the world involves ultrasonic techniques. B-scan images have good spatial resolution (better than a millimeter in abdominal scanning), good tissue contrast and can be formed in real-time. One of the disadvantages of these images is the presence of speckle noise, which is caused by the interference between the backscattered ultrasonic waves in soft tissues. This noise is present in laser, sonar and synthetic aperture radar (SAR) imagery. Speckle pattern reduces the target detectability in B-scan images. It does not affect contrast resolution though it does reduce the useful spatial resolution. The reduction affects the human ability to identify normal and pathological tissues.

Speckle noise has been widely studied, mainly with an stochastic approach within the framework of statistical optics (Goodman, 1985) due to its non-deterministic nature. Many filters have been proposed using the statistical nature of this noise. Deterministic or model-free filters have also been tried, with limited success so far (WFUMB, 1997).

Most speckle filters have been proposed and assessed in remote sensing applications (Oliver and Quegan, 1998). These filters can be classified into linear and non-linear depending on the operations they use, or according to the framework they employ (local, global, adaptive, robust (Frery *et al.*, 1997b), maximum a posteriori etc.). A comprehensive survey of speckle filters for remote sensing applications can be found in Lee *et al.* (1994).

Speckle suppression in ultrasonic imaging is usually done by adding uncorrelated images of the scan plane (a technique called *multilook* by the remote sensing community), by adaptive filtering in the spatial domain (Bamber and Draft, 1986), or by processing in the wavelet domain (Rakotomamonjy *et al.*, 2000).

Though there is no consensus in the definition of "good" filters, it is clear that the application at hand requires procedures that, simultaneously, reduce the noise and retain the main features of the images. Medicine practitioners are used to discover important tissue characteristics in ultrasound imagery under the presence of speckle noise. Nevertheless, the increasing of the signal-to-noise relation might have a potential impact on their ability of recognizing normal and pathological tissues.

In this work, some of the most popular filters (Mean, Median, Lee, Frost and MAP) are reviewed and applied to ultrasound B-scan images (Lee, 1986), along with a non-linear technique based on medians applied to the binary slice images. The performance of these filters is assessed both quantitatively (regarding noise suppression and radiometric preservation) and qualitatively (through perceptual contrast and edge preservation) using both real and simulated data.

II. IMAGE FORMATION AND SPECKLE FILTERS

In the following, a short description of the filters employed in this paper is presented. The application here studied, namely B-scan images, has specific requirements that guide the choice of filters to be assessed. Data have to be shown as collected, therefore, on-line processing is required. The practitioner that is operating the equipment should not be distracted by the complexity of the operation. Thus, the filters must require minimum interaction and parameters specification.

The criteria used to choose the techniques here studied were

1. their popularity among remote sensing users,
2. their ease of implementation and use (which prohibited the use of filters based on simulated annealing (Oliver and Quegan, 1998), for instance), and
3. their computational requirements (disregarding those that demand specialized hardware).

One of the most complete models for image formation was proposed by Geman and Geman in 1984 (Geman and Geman, 1984) and extended by Bustos and Frery (1992). This model, when restricted to real-valued images, postulates the existence of a non-observed image $\mathbf{X}\colon S \to \mathbb{R}$ that suffers from blurrings $\mathbf{H} = (H_s)_{s\in S}$ and from typically non-linear invertible distortions $\phi = (\phi_s)_{s\in S}$, $\phi_s\colon \mathbb{R} \to \mathbb{R}$. The support S may have any structure, but the most common in this kind of application is the Euclidean grid of the form $S = \{0, \dots, m-1\} \times \{0, \dots, n-1\}$. The blurrings are operations defined as $H_s\colon \mathbb{R}^{p_s} \to \mathbb{R}$, where p_s is the number of pixels involved in the computation of the blurred value in site $s \in S$.

Once the image has been degraded by these two deterministic operators, a noise field η enters in scene through a set of invertible pointwise operations $\odot = (\odot_s)_{s\in S}$. In this manner, the observed image $\mathbf{Z}$ is given by

$$\mathbf{Z} = \phi(\mathbf{H}(\mathbf{X}))\odot \eta. \qquad (1)$$

Given a corrupted image $\mathbf{z}$, any restoration will take the form of an estimator of the true process $\mathbf{x}$. Thus, we denote it by $\hat{\mathbf{x}}$.

It has been shown (Abbou and Thurstone, 1979) that the speckle present in the enveloped-detected signal (RF amplitude signal) of ultrasound images is a kind of multiplicative noise. Furthermore, amplitude speckled images are conveniently modelled assuming that there is neither blurring nor distortion, and that the noise obeys a square-root-of-Gamma law. Considering multiplicative noise, Eq. (1) can be simplified to $\mathbf{Z} = \mathbf{X} \cdot \eta$, where $\eta = (\eta_s)_{s\in S}$ are independent identically distributed random variables whose distributions are characterized by the density

$$f_\eta(y) = \frac{n^n}{\Gamma(n)} y^{2n-1} \exp\left(-ny^2\right), n, y > 0,$$

where n is known as number of looks and depends on how the image was processed. The $n = 1$ case, which amounts to the Rayleigh distribution and fully developed speckle, is usually accepted for the application here studied. Fig. 1 shows densities of this distribution for the single look ($n = 1$) and two multilook ($n = 3$ and $n = 8$) cases. It is noticeable that the smaller the number of looks the more skewed the density.

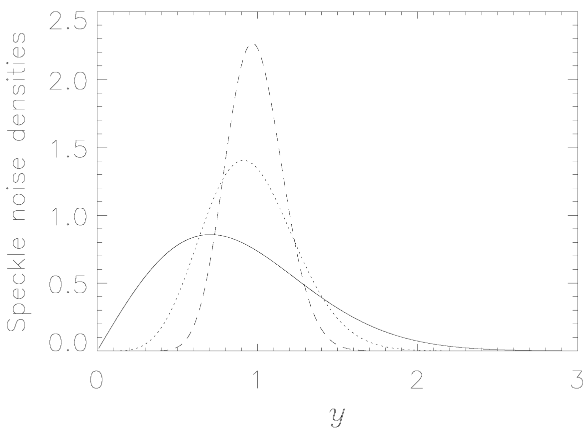

Figure 1: Speckle noise densities for the $n \in \{1, 3, 8\}$ looks cases (solid line, dots, dashes, respectively).

This modelling requires the random field $\mathbf{X}$ to take positive values; these values are regarded as the unobserved truth, and they are called *backscatter* by the SAR remote sensing community.

The multiplicative model for speckle statistics only concerns RF data. Several kinds of processing for RF data, such as preamplification and dynamic range reduction (logarithm or linear compression, for instance), is performed before displaying images. Our experiments with real images was done using an equipment with linear compression for dynamic range. Despite the processing on the RF data for displayed images, the experimental set-up with linear compression is in a fair agreement with the multiplicative model and speckle noise square-root-of-Gamma law.

A real and a simulated image were extensively used in this experience. The former was taken over the testicles of a patient suffering filariasis (Amaral *et al.*, 1994), and is shown in Fig. 2 (left). An experienced physician is able to detect a parasite as a small light dot in the middle of the dark spot in the center of the image. The synthetic data is a phantom used to assess the performance of image processing techniques from the standpoint of small details preservation. It consists of light strips and dots over a dark background, and is shown in Fig. 2 (right); it is of one-look noise multiplied by the true values.

In the next sessions, we quickly review the filters chosen for the assessment.

A. Mean Filter

The local mean can be used whenever there is noise in an image. It has the nice properties of locally reducing the variance (increasing, thus, the signal-to-noise ratio) and of being of trivial implementation and use (requiring the user to specify only the size of the window). It is the simplest non-trivial case of convolution, but it has the effect of potentially blurring the image. It is also possible to see that this filter is optimal for additive Gaussian noise (regarded as the "classical" model), but it is quite inefficient when the data defy this hypothesis. It is known that speckled images obey a multiplicative model with non-Gaussian noise (Frery *et al.*, 1997a) and, therefore, it is expected that the simple mean is not the optimal choice in this case.

B. Median Filter

This filter outperforms the mean when the image is affected by impulsive noise, i.e., when $\eta = (\eta_s)_{\mathbf{s}\in\mathbf{S}}$ are independent identically distributed random variables whose distributions are characterized by the law $\Pr(\eta_s = M) = 1 - \Pr(\eta_s = 0) = \epsilon < 1/2$. In this equation, M is a "huge" number and additions are the pointwise operations. This model frequently appears in robustness studies, and in the modelling of corner reflectors in SAR imagery (Bustos *et al.*, 2002).

When the classical model (additive Gaussian noise) is correct, this filter is less effective in combating the noise than the mean. Neverthless, whichever the true model, the median produces less blurred images. Compound procedures that use both the mean and the median are also possible.

C. Median-filtered binary slices (MFBS)

Byte images can be decomposed in eight bit images, that can be conveniently treated with binary tools as those provided by mathematical morphology (Serra, 1988). Consider the observed byte image $\mathbf{z}\colon S \to \{0,\dots,255\}$; every observed value $z(s)$ can be written as an eight bits string, i.e., $z(s) = (b_0(s)b_1(s)\dots b_7(s))$, with $b_i \in \{0,1\}$ for every $0 \le i \le 7$ and every $s \in S$.

This decomposition allows writing the observed gray scale image as an stack of eight binary images called *slices*: $\mathbf{z} = (\mathbf{z}_0, \mathbf{z}_1, \dots, \mathbf{z}_7)$, where $\mathbf{z}_i\colon S \to \{0,1\}$ for every $0 \le i \le 7$.

Binary filters, one of the specialities of mathematical morphology, can be then applied to each slice. The resulting image is the stacking of the treated binary slices: $\hat{\mathbf{x}} = (\Psi_0(\mathbf{z}_0), \Psi_1(\mathbf{z}_1), \dots, \Psi_7(\mathbf{z}_7))$, where Ψ_i is a binary transformation. In this work the median will be used as Ψ_i for every slice.

Techniques based on mathematical morphology have also been used to improve classification results in remote sensing data (Frery and Candeias, 1994).

D. Lee and Frost filters

These adaptive filters use local statistics (prior mean, variance and spatial correlation) in order to alleviate the blurring effect of the mean and, at the same time, to reduce speckle more effectively than the median (Lee *et al.*, 1994).

The Lee filter computes a minimum mean square estimate of the true signal using a linear filter. The resulting equation only needs knowledge of the noise variance which depends on the processing, i.e., on the number of looks, and is usually known or easily estimated.

The Frost filter is the Wiener estimate of the true signal using local statistics; the correlation function is assumed to decay exponentially with the distance.

E. Maximum a posteriori (MAP) filters

MAP filters require assumptions about the distribution of the true process and of the degradation model. A MAP estimate, when available, is the solution of $\arg\max_{\mathbf{X}} \Pr(\mathbf{X} \mid \mathbf{Z})$ where $\mathbf{X}$ is the unobserved truth and $\mathbf{Z}$ the model for the observed data. Using Bayes' theorem one can write $\Pr(\mathbf{X} \mid \mathbf{Z}) \propto \Pr(\mathbf{Z} \mid \mathbf{X}) \Pr(\mathbf{X})$ where "$\propto$" denotes proportionality, $\Pr(\mathbf{X})$ is the model for the truth and $\Pr(\mathbf{Z} \mid \mathbf{X})$ explains how the truth is converted into observed data. Different assumptions for the distribution of $\mathbf{X}$ and for the degradation lead to different MAP estimators with different associated complexities. Gaussian distributions were assumed, since this hypothesis leads to feasible solutions.

III. FILTER ASSESSMENT

Two quantitative criteria were used to assess the performance of the filters: signal-to-noise relation and radiometric preservation. A qualitative evaluation was also performed. This filter assessment aims at deciding which is the best filter for the application at hand and, simultaneously, at finding the optimal set of parameters. The filters were applied in an iterative manner, so their performances are reported for the first, second and third iteration. The windows used were of size 3×3, 5×5, 7×7 and 9×9.

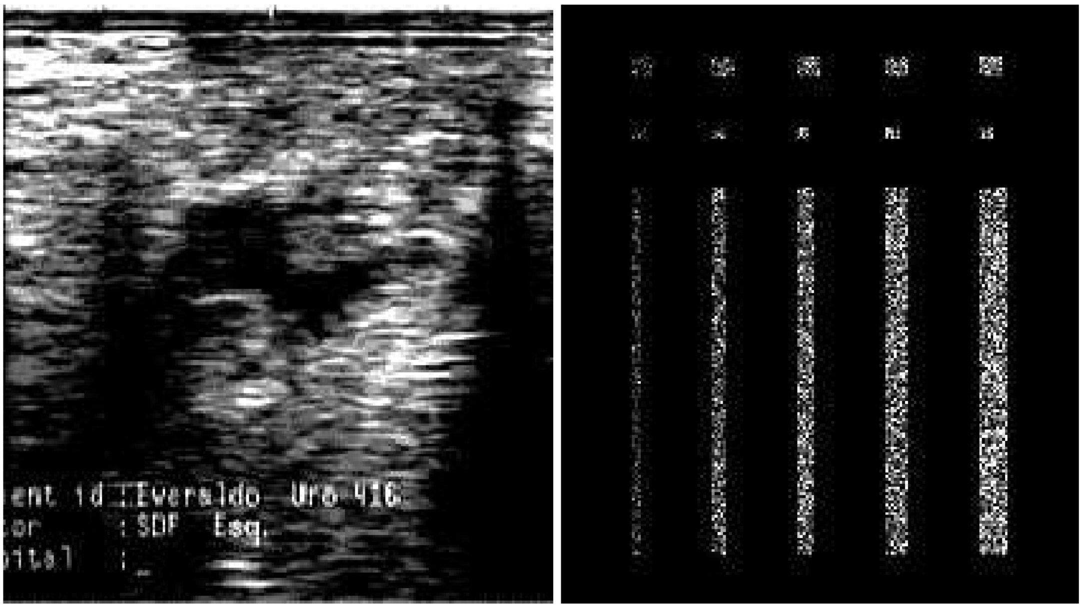

Figure 2: Original (left) and simulated (right) ultrasound images.

The signal-to-noise relation was here assessed using the speckle suppression metric, proposed by Xie *et al.* (1999) and defined as $F = s_{\mathbf{z}} m_{\hat{\mathbf{x}}}/(s_{\hat{\mathbf{x}}} m_{\mathbf{z}})$, where s and m denote sample standard deviation and mean, respectively.

The radiometric preservation was assessed through the normalized mean square error, also proposed by Xie *et al.* (1999). It is computed over a homogeneous area $A \subset S$ with mean μ as $\sum_{s \in A}(\hat{x}(s) - \mu)^2/(\#A\mu)$, where $\#A$ denotes the number of elements of the set A. The smaller this metric the better the performance of the filter.

The qualitative analysis was applied in two stages: the first to the filtered versions of the synthetic image, since it is possible to compare them with the truth; the second to the filtered versions of the real images. The former consisted in finding the number and precision of objects (spots and lines) remained after filtering, while the latter required a subjective evaluation of how "better" or "worse" the result is compared to the original (unfiltered) image.

In the following, we present the results of our assessment.

A. Speckle suppression

Using the smallest window the best filter under this criterion was the mean, followed by Lee and Frost. Using 5×5 windows the best speckle suppressions were attained by the mean, median and Frost, in decreasing order. When 7×7 and 9×9 windows where used the best filters were the mean, median and MFBS.

This metric did not exhibit a variation proportional to the window size, as was expected. The mean and Lee filters were the ones for which there is a noticeable performance increase after the first iteration.

B. Normalized mean square error

Two different samples were chosen to measure this quantity: and edge and a small spot. In every case the Frost filter was the one with best performance, followed by the Lee and median filters.

C. Qualitative assessment

The Lee filter preserved all the details in every situation, though its performance in combating the noise is limited, from the visual standpoint. The Frost filter preserved better the linear features than the small spots, but it produces smoother images. The MFBS preserved only the linear features; the mean suppressed four out of sixteen features and the blurring it imposes was negatively assessed by the users. The median filter has a similar behavior to the mean, with the difference that it preserves better the edges. The MAP filter was good at preserving details but, similarly to the Lee filter, its impact on noise intensity is limited.

The Frost filter was consistently considered to produce better images than the original one, at any widow size, followed by the Lee filter, by the median and the mean. These last two filters blurred the images to an extent considered unacceptable by the final users, though they all pointed that the noise suppression is remarkable.

IV. CONCLUSIONS AND FUTURE WORK

The data at hand was better processed by the Frost filter with window sizes of 3×3, 5×5, 7×7 and 9×9, from both quantitatively and qualitatively criteria. This suggests the use of this filter in the practice of ultrasound B-scan imaging, allowing the user to control the window size in order to choose between blurring and noise suppression. This filter is computationally affordable and easy to implement. Fig. 3 shows the result of applying the 5×5 Frost filter over the original image.

Figure 3: Frost 5×5 filtered image.

The distributions associated to the multiplicative model (see Frery *et al.*, 1997a) were not consistently observed in the data at hand. This is possibly due to the fact that discarding the distorting functions ϕ in Eq. (1) is not realistic, a fact that may have major impact in the performance of MAP filters. This will be further investigated on RF data, and better adapted filters will be proposed and assessed.

Hardware/software co-design techniques are being used to make optimal partitioning of the procedures.

ACKNOWLEDGMENTS

The authors are grateful to CNPq for partial funding of this work.

REFERENCES

Abbou, J. and F. Thurstone, "Acoustic speckle: Theory and experimental analysis," *Ultrasonic Imaging* **1**, 303–324 (1979).

Amaral, F., G. Dreyer, J. Figueiredo-Silva, J. Norões, A. Cavalcanti, S.C. Samico, A. Santos and A. Coutinho, "Live adult worms detected by ultrasonography in human bancroftian filariasis," *Amer. J. of Tropical Medicine* **50**, 753–757 (1994).

Bamber, J.C. and C. Draft, "Adaptative filtering for the reduction of speckle in ultrasonic pulse-echo images," *Ultrasonics* **24**, 41–43 (1986).

Bustos, O.H. and A.C. Frery, "A contribution to the study of Markovian degraded images: an extension of a theorem by Geman and Geman," *Comput. Appl. Math.* **11**, 17–29, 281–285 (1992).

Bustos, O.H. M.M. Lucini and A.C. Frery, "M-estimators of roughness and scale for GA0-modelled SAR imagery," *EURASIP J. Appl. Signal Processing* **2002**, 105–114 (2002).

Frery, A.C. and A.L.B. Candeias, "On the improvement of 1-look SAR image segmentations with mathematical morphology," In *Image and Signal Processing for Remote Sensing* SPIE **2315**, 245–255 (1994).

Frery, A.C., H.-J. Müller, C.C.F. Yanasse and S.J.S. Sant'Anna, "A model for extremely heterogeneous clutter," *IEEE Trans. Geosc. Rem. Sens.* **35**, 648–659 (1997a).

Frery, A.C., S.J.S. Sant'Anna, N.D.A. Mascarenhas and O.H. Bustos, "Robust inference techniques for speckle noise reduction in 1-look amplitude SAR images," *Appl. Signal Processing* **4**, 61–76 (1997b).

Geman, D. and S. Geman, "Stochastic relaxation, Gibbs distributions and the Bayesian restoration of images," *IEEE Trans. Patt. An. Mach. Intel.* **6**, 721–741 (1984).

Goodman, J.W., *Statistical Optics*, Wiley, New York (1985).

Lee, J.S., "Speckle suppression and analysis for synthetic aperture radar images," *Optical Engineering* **25**, 636–643 (1986).

Lee, J.S., I. Jurkevich, P. Dewaele, P. Wambacq and A. Oosterlink, "Speckle filtering of synthetic aperture radar images: a review," *Rem. Sens. Rev.* **8**, 313–340 (1994).

Oliver, C. and S. Quegan, *Understanding Synthetic Aperture Radar Images*, Artech, Boston (1998).

Rakotomamonjy, A., P. Deforge and P. Marché, "Wavelet-based speckle noise reduction in ultrasound B-scan images," *Ultrasound Imaging* **22**, 73–94 (2000).

Serra, J.P.F, *Image Analysis and Mathematical Morphology: Theoretical Advances*, v. 2., Academic, London (1988).

World Federation for Ultrasound in Medicine and Biology News, *Ultrasound in Medicine and Biology* **4**, 974 (1997).

Xie, H., F.T. Ulaby, L.E. Pierce and M.C. Dobson, "Performance metrics for SAR speckle-suppression filters", In *IGARSS*, IEEE, CD-ROM (1999).

Received: June 11, 2002.
Accepted for publication: December 20, 2002.
Recommended by Subject Editor Ricardo S. Sánchez Peña.